Supporting Information

Trans-interfacial distribution of Se vacancies in Bi_2Se_3 core and carbon nanofiber matrix enables long-lifespan and ultra-stable sodium storage

Faxiu Zhang[a], Jing Xie[a*], Xinxin Yin[a], Gaoyuan Liu[a], Zhenjiang Lu[a], Jindou Hu[a], Yong Wen[b*], Yali Cao[a*]

[a]*State Key Laboratory of Chemistry and Utilization of Carbon Based Energy Resources, College of Chemistry, Xinjiang University, Urumqi 830017, Xinjiang, PR China.*
[b]*School of Civil Engineering and Architecture, Xinjiang University, Urumqi 830017, China*

*Corresponding author.
E-mail address: caoyali523@163.com (Y. Cao); xiejing@xju.edu.cn (J. Xie); wenyong_9731@126.com

Methods

1. Material characterizations

X-ray diffraction (XRD, SmartLab-SE, 40 kV, Cu−Kα Radiation, λ = 0.154 nm) and X-ray photoelectron spectroscopy (XPS, Thermo Scientific K-Alpha) were employed for the phase characterization of the samples. Morphology and structural characterization were performed using field−emission scanning electron microscopy (FESEM, Hitachi S-4800) and transmission electron microscopy (TEM, JEOL JEM-2100F). Raman spectroscopy testing was conducted using a Xplora Plus. Electron paramagnetic resonance (EPR) spectra obtained using a Bruker W500 spectrometer. Nitrogen adsorption-desorption isotherm and Brunauer-Emmett-Teller (BET) surface area measurements were conducted at 77 K using a Micromeritics ASAP 2460 instrument. The carbon content of Bi_2Se_{3-x}@CNFs composite material was analyzed using thermogravimetric analysis (TGA, Hitachi STA7300) from 30 to 800 ℃ in air with a heating rate of 10 ℃ min^{-1}.

2. Electrochemical measurements

The electrochemical properties of the as-obtained samples were assessed using CR2032 half-cells, which were assembled in an Ar-filled glove box. The working electrode was prepared by mixing the active material, Super P, and polyvinylidene fluoride (PVDF) in a mass ratio of 7:2:1 in N-methyl-2-pyrrolidone (NMP). Then, the slurry was uniformly coated onto a copper foil and vacuum-dried at 70 ℃ for 12 hours. The electrode was punched into disks with a diameter of 12 mm. The half-cell assembly included sodium metal as the counter electrode, a Whatman GF/D glass fiber as the separator, and 1 M $NaPF_6$ in DME as the electrolyte. The assembly of full cells involved using Bi_2Se_{3-x}@CNFs as the anode material and $Na_3V_2(PO_4)_3$ mixed with Super P and polyvinylidene fluoride (PVDF) in an 8:1:1 ratio, coated on aluminum foil as the cathode material and assessed within a voltage range of 0.8-3.8 V. Galvanostatic charge-discharge (GCD) tests and galvanostatic intermittent titration technique (GITT) measurements were performed on a LAND CT-2001A battery

testing system within a voltage window of 0.01-3.0 V(vs. Na^+/Na). Cyclic voltammetry (CV) and electrochemical impedance spectroscopy (EIS) tests were conducted on the CHI 660E electrochemical workstation (Chenhua Instrument Company, Shanghai, China). The CV tests were performed at scan rates ranging from 0.1 to 1 mV s^{-1}, while the EIS measurements were taken over a frequency range of 10^5 Hz to 10^{-2} Hz.

3. Calculation process for Bi_2Se_3 content in Bi_2Se_{3-x}@CNFs from TGA analysis

The content of Bi_2Se_3 in Bi_2Se_{3-x}@CNFs was determined by thermogravimetric analysis (TGA). The weight increment of Bi_2O_3, generated by the oxidation of Bi_2Se_3 ($2Bi_2Se_3 + 10O_2 + C \rightarrow 2Bi_2O_3 + CO_2\uparrow + 6SeO_2\uparrow$), was analyzed based on the weight loss due to carbon combustion (Figure S3b). According to the reaction equation, the weight loss of pure Bi_2Se_3 to form Bi_2O_3 is 28.9%. Therefore, the content of Bi_2Se_3 in Bi_2Se_{3-x}@CNFs can be calculated by the following formula:

$$X * 28.9\% + (100 - X) = 86.4\% \quad \text{(S1)}$$

where X represents the loading content of Bi_2Se_3, and the loading content of carbon is (100%-X). From this, it can be calculated that the content of Bi_2Se_3 in Bi_2Se_{3-x}@CNFs-600 is 18.8%.

4. The calculation process for the pseudocapacitive contribution:

The measured current of the CV curves can be attributed to two types of charge storage mechanisms for electrode materials. Typically, the kinetics of charge storage can be explored through the power-law relationship between the measured current density (i) and the sweep rate (v), which is described by the following equations:

$$i = av^b \quad \text{(S2)}$$

$$log(i) = blog(v) + log(a) \quad \text{(S3)}$$

in these equations, a and b are variables. Specifically, the b-value of 0.5 indicates a purely faradaic intercalation process, while the b-value of 1 signifies an ideally capacitive contribution process. Quantitatively, the mixed behaviors can be further distinguished by separating the current response (i) at a specific potential (V), as

described by the following equations:

$$i(v) = k_1 v + k_2 v^{1/2} \quad \text{(S4)}$$

where $k_1 v$ and $k_2 v^{1/2}$ represent the contributions of the capacitive and diffusion behaviors, respectively.

5. DFT method

All the computations were carried out by spin-polarized DFT method, as implemented in Vienna ab initio Simulation Package (VASP 5.4.4). The exchange correlation energy was modeled by the Perdew−Burke−Ernzerhof (PBE) functional within the generalized gradient approximation (GGA). An energy cutoff of 450 eV was adopted for the plane-wave basis. In structural optimizations, the energy and force convergence thresholds were set to 10^{-5} eV and 0.05 eV/Å, respectively. The Brillouin zone was sampled by 2 × 2 × 1 k-points using the Monkhorst−Pack scheme. we constructed 3×3×1 supercells from the unit cells of Bi_2Se_3 and 5×5×1 supercells from graphene to build heterostructures. A vacuum of 30 Å along the z-direction was fixed to avoid interaction between adjacent layers. Visualization was performed using VESTA, and postprocessing of the VASP data was conducted with VASPKIT.

Supplementary Figures and Tables

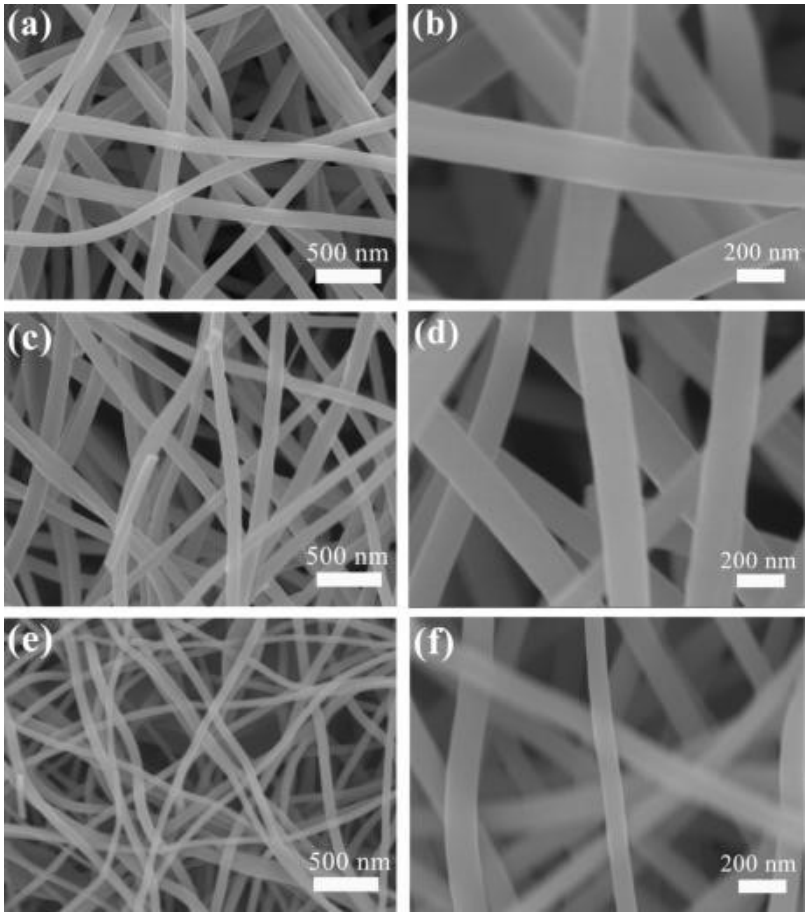

Fig. S1. SEM images of (a, b) Bi_2Se_{3-x}@CNFs-500, (c, d) Bi_2Se_{3-x}@CNFs-700 and (e, f) CNFs.

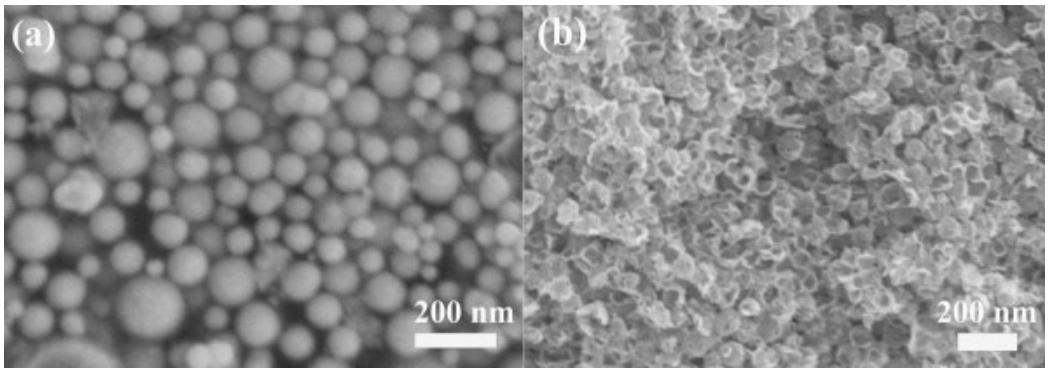

Fig. S2. SEM images of (a) Bi PNS and (b) Bi_2Se_3.

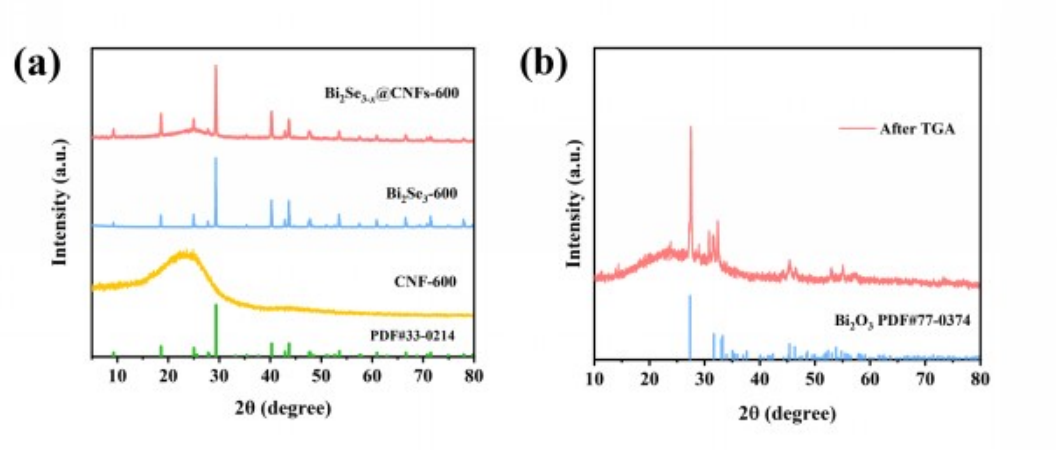

Fig. S3. (a) XRD patterns of Bi_2Se_{3-x}@CNFs-600, Bi_2Se_3-600 and pure CNF, (b) XRD pattern of Bi_2Se_{3-x}@CNFs-600 residue after the TGA test.

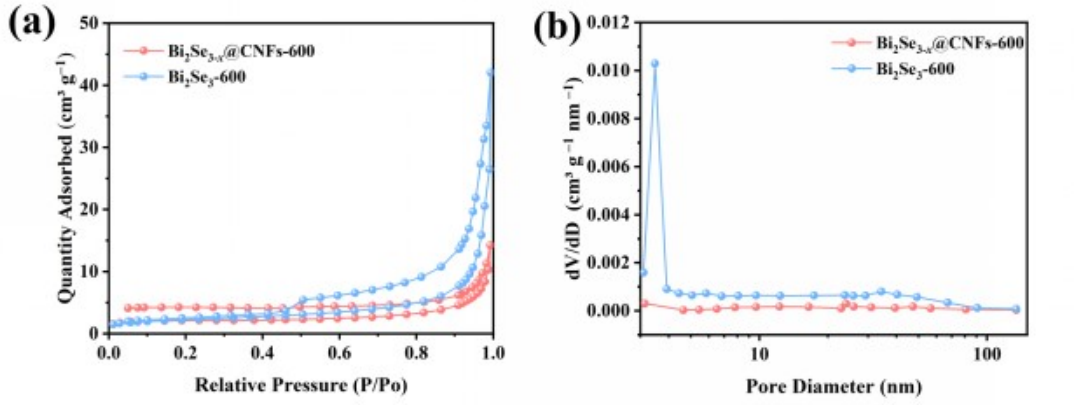

Fig. S4. (a) N_2 adsorption-desorption isotherms and (b) Pore size distribution profiles of Bi_2Se_{3-x}@CNFs-600 and Bi_2Se_3-600.

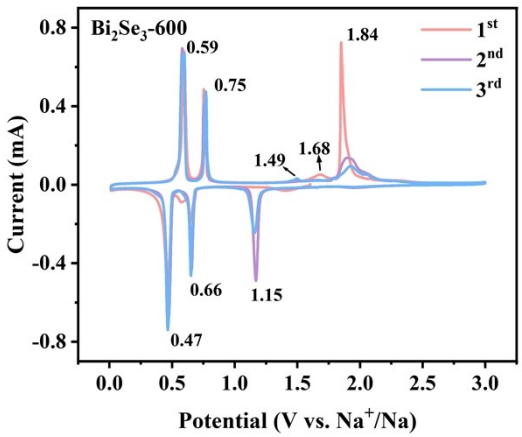

Fig. S5. CV curves of Bi_2Se_3-600 at 0.1 mV s^{-1}.

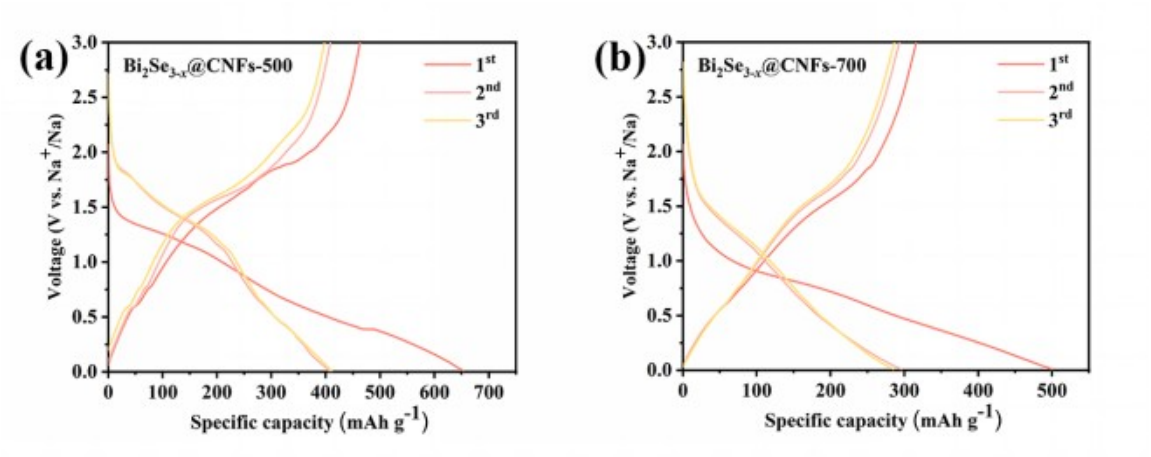

Fig. S6. GCD profiles at 0.1 A g^{-1} of (a) Bi_2Se_{3-x}@CNFs-500 and (b) Bi_2Se_{3-x}@CNFs-700.

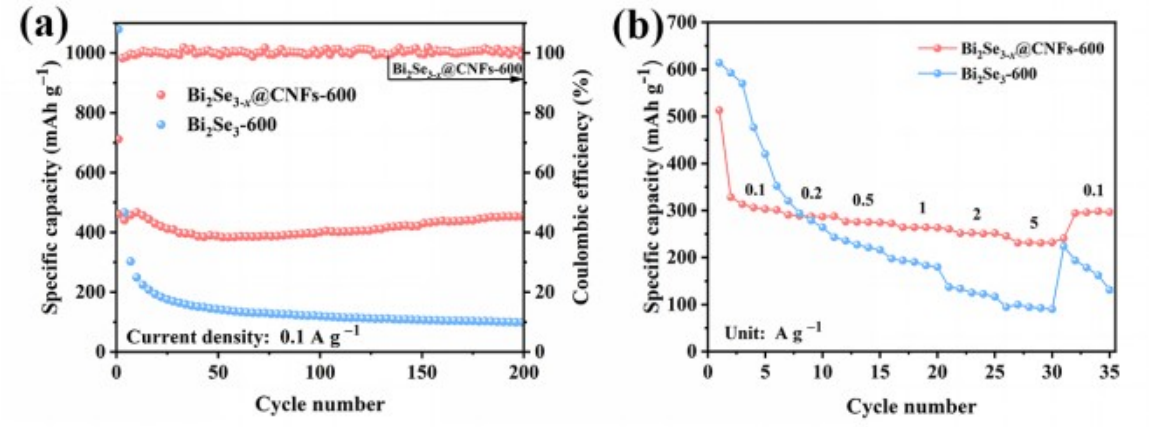

Fig. S7. (a) Cycling performance at 0.1 A g^{-1}, (b) rate performance of Bi_2Se_{3-x}@CNFs-600 and Bi_2Se_3-600.

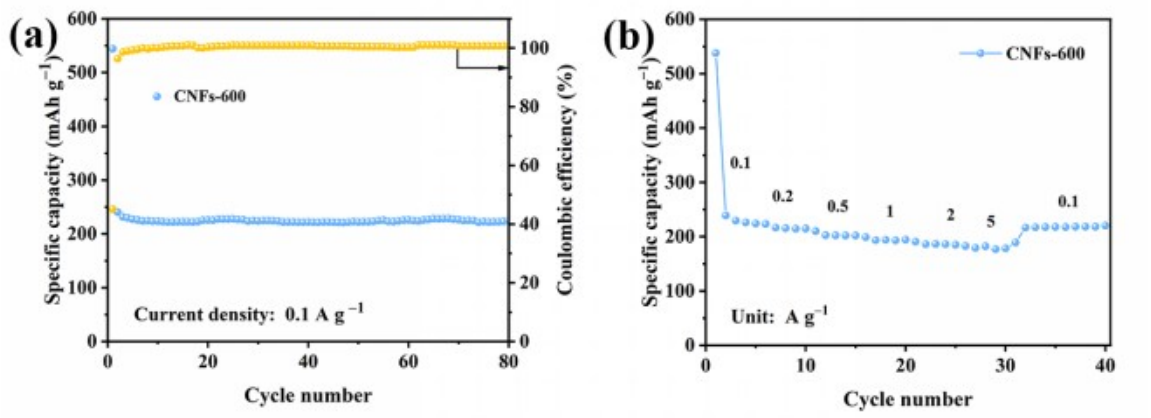

Fig. S8. (a) Cycling performance at 0.1 A g^{-1}, (b) rate performance of CNFs-600.

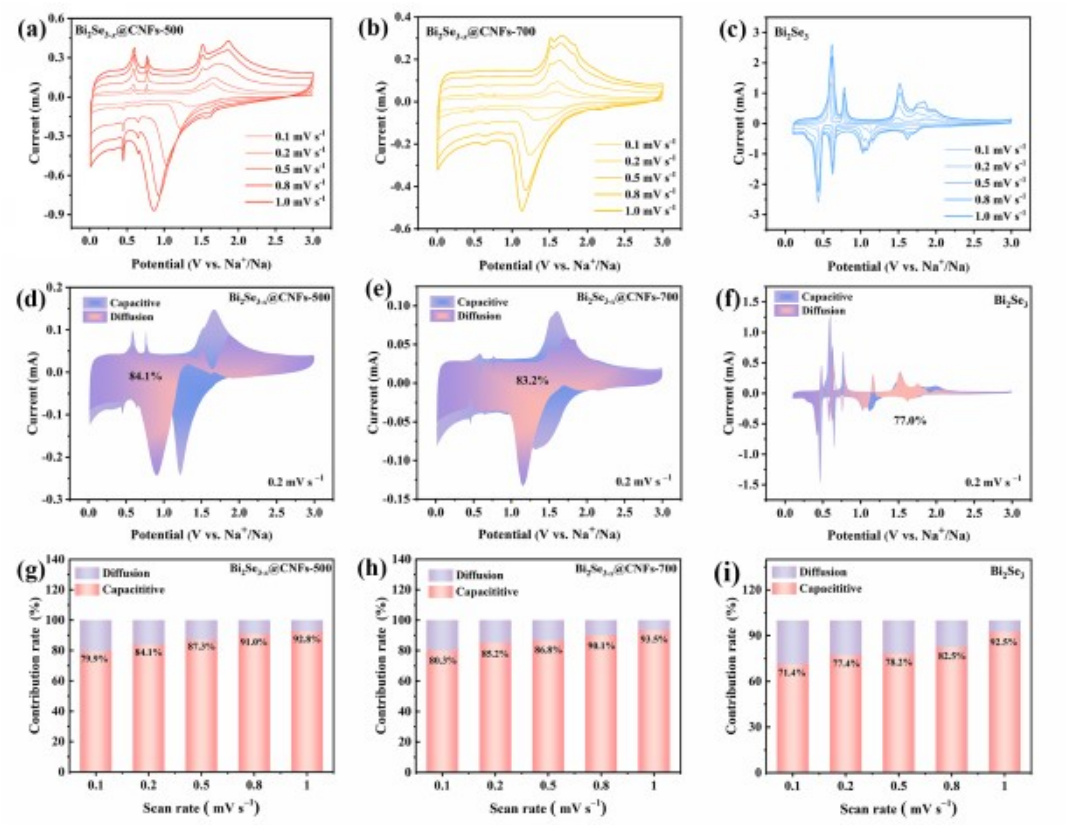

Fig. S9. (a-c) CV curves at various scan rates. (d-f) Capacitive contribution at 0.2 mV s^{-1}. (g-i) Capacitive contribution ratios of Bi_2Se_{3-x}@CNFs-500, Bi_2Se_{3-x}@CNFs-700 and Bi_2Se_3 at various scan rates.

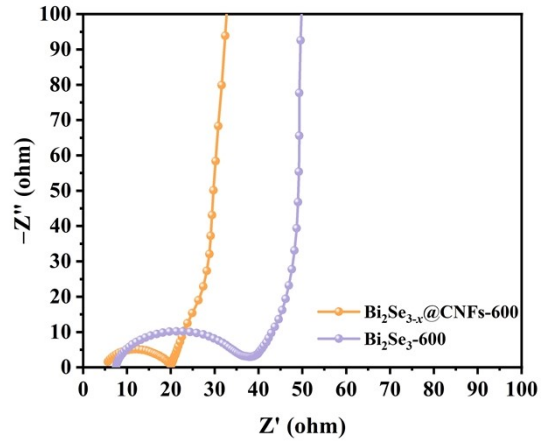

Fig. S10. Nyquist plots of Bi_2Se_{3-x}@CNFs-600 and Bi_2Se_3-600.

Table S1. The electrochemical performance comparison of Bi_2Se_{3-x}@CNFs-600 with other reported Bi_2Se_3-based anode materials.

Sample	Curret density ($A\ g^{-1}$)	Cycles	Capacity after cycling ($mAh\ g^{-1}$)	Ref.
Bi_2Se_3/NG-7	1	129^{th}	254.5	[1]
G-Bi_2Se_3/C	0.1	100^{th}	375.3	[2]
Bi_2Se_3-C/G-1	2	1000^{th}	241	[3]
Bi_2Se_3/Bi_2O_3	0.1	100^{th}	310	[4]
Bi_2Se_3 nanocrystal	1	200^{th}	210.2	[5]
Bi_2Se_{3-x}@DNC	5	1500^{th}	253.4	[6]
Bi_2Se_3@NC(Co)	5	500^{th}	238	[7]
Bi_2Se_{3-x}@CNFs-600	5	3000^{th}	284	This work

References

[1] W.Liang, B. Chen, W. Lin, L. Shao, X. Shi, Z. Sun, *Mater. Lett.*, 2023, **332**, 133542.

[2] B. He, J. Cunha, Z. Hou, G. Li, H. Yin, *J. Colloid Interface Sci.*, 2023, **650**, 857–864.

[3] D. Li, J. Hu, C. Wang, L. Guo, J. Zhou, *J. Power Sources*, 2023, **555**, 232387.

[4] M. Han, Z. Zhou, Y. Li, Q. Chen, M. Chen, *J. Alloys Compd.*, 2022, **892**, 162143.

[5] S. Dai, L. Wang, Y. Shen, M. Wang, *Appl. Mater. Today*, 2020, **18**, 100455.

[6] Z. Lin, W. Zhang, J. Peng, Q. Li, Z. Liang, G. Wang, J. Wang, G. Wang, Z. Huang, S. Huang, *Adv. Energy Mater.*, 2024, **14**, 2402110.

[7] X. Liu, S. Zhang, Z. Duan, X. Guo, Y. Liu, X. Zheng, Q. Fan, Q. Kong, J. Zhang, *J. Power Sources*, 2025, **649**, 237471.